John von Neumann Institute for Computing

Free Energy and Rare Events in Molecular Dynamics

Nikos L. Doltsinis

published in

Computational Nanoscience: Do It Yourself!,
J. Grotendorst, S. Blügel, D. Marx (Eds.),
John von Neumann Institute for Computing, Jülich,
NIC Series, Vol. **31**, ISBN 3-00-017350-1, pp. 375-387, 2006.

http://www.fz-juelich.de/nic-series/volume31

Free Energy and Rare Events in Molecular Dynamics

Nikos L. Doltsinis

Chair of Theoretical Chemistry
Ruhr-Universität Bochum
44780 Bochum, Germany
E-mail: nikos.doltsinis@theochem.rub.de

Molecular dynamics (MD) preferentially samples regions of configuration space close to potential minima while transition state regions at the top of high reaction barriers are rarely visited. In this lecture, we will discuss a variety of improved sampling techniques that make possible the study of rare events on the finite MD time scale and the calculation of free reaction energies.

1 Introduction

Any kind of molecular dynamics (MD) simulation, be it classical (i.e. using force fields) or *ab initio*, suffers from the same fundamental limitations due to the finiteness of computational resources. Although the arguments and computational techniques presented in this article apply to both types of MD, our perspective is that of a first principles dynamicist.

Despite continuous advances in both numerical efficiency and computer technology, Car-Parrinello molecular dynamics (CP-MD) simulations[1,2] are still limited to processes involving a few hundred atoms and occurring within a few tens of picoseconds at most. The number of chemical reactions which take place spontaneously on such a short time scale, however, is fairly limited; typically energy barriers of many kcal/mol need to be overcome. A wide variety of computational approaches have been developed over the years to force or speed up chemical reactions in ab initio molecular dynamics and calculate free energies.

The fundamental problem in moving from reactants to products is that the true reaction coordinate is often unknown. Choosing a realistic reaction coordinate is essential for a simulation of rare events to be useful. This task becomes exceedingly difficult for systems with large numbers of nuclear degrees of freedom. A way of systematically determining an ensemble of reaction coordinates has been suggested by Chandler and co-workers[3,4] based on pioneering work by Pratt[5]. Although powerful and appealing, their transition path sampling method is computationally rather demanding, in particular when used in combination with CP-MD[6]. In the latter context, a variety of alternative methods has been proposed over the years. One class of approaches is based on geometric constraints, such as simple atomic distances[7,8], collective "target" distance[9–12] or coordination number[13–16] constraints. The strategy of another class of methods is to suitably modify the potential energy surface to enhance sampling of rare events. Chemical flooding[17], adiabatic free energy sampling[18,19] and non-Markovian metadynamics[20–24] all fall into this category.

The present article will cover aspects of both classes of methods, the focus being on the frequently used constraint techniques. After a general introduction to the constraint formalism in MD, we will describe in some detail two specific constraint approaches, the coordination constraint and the targeted MD (TMD) methods. In the last part of this text, the method of non-Markovian metadynamics shall be presented.

In a limited number of cases, the reaction coordinate can be approximated reasonably well by simple geometric variables, such as bond lengths or angles. Rare events of this type may be studied using standard constraint techniques[25–28], provided that one is able to guess the reaction mechanism prior to the simulation.

For cases where the reaction coordinate cannot be well approximated by such simple constraints, i.e. for complex reactions involving a large number of atoms, there exist a number of more advanced constraint methods. The coordination number constraint, for instance, was designed by Sprik[13–16] to describe chemical reactions in solution. Despite being a simple scalar order parameter, the coordination constraint is capable of acting on all atoms in the system. Thus it ensures a large degree of intrinsic flexibility while retaining the numerical simplicity of a simple bond constraint.

Similarly, the TMD approach proposed by Schlitter and co-workers[9–11] can be treated using the well-established numerical techniques developed for standard distance constraints without the need to know in advance a good low-dimensional approximation to the reaction coordinate. In the TMD method, the reaction coordinate is defined by a single mass-weighted root-mean-square "target distance" between a known initial structure and a fixed final (target) structure. By gradually reducing the constrained target distance to zero, the system is driven from the reactant to product state without explicitly defining the reaction pathway.

The method of non-Markovian metadynamics[20–23] is based on the idea that the system can be forced to sample higher-energy regions of configuration space by gradually filling up the wells of the potential energy surface. This is achieved by adding an artificial Gaussian-shaped contribution to every region that is visited during the simulation thereby driving the system out of one local minimum to a neighboring local minimum.

2 Constraint Techniques

2.1 Basic Theory

2.1.1 Constrained Molecular Dynamics

The Lagrangian of an unconstrained system consisting of N atoms with positions $\mathbf{R} = (\mathbf{R}_1, \mathbf{R}_2, \ldots, \mathbf{R}_K, \ldots, \mathbf{R}_N)$ and masses M_K is

$$\mathcal{L} = \mathcal{T} - \mathcal{V} = \frac{1}{2}\sum_{K}^{N} M_K \dot{\mathbf{R}}_K^2 - \mathcal{V}(\mathbf{R}) \tag{1}$$

where $\mathcal{T}$ and $\mathcal{V}$ are the kinetic and potential energies, respectively. The equations of motion

$$\frac{\partial}{\partial t}\frac{\partial \mathcal{L}}{\partial \dot{R}_K^\alpha} = \frac{\partial \mathcal{L}}{\partial R_K^\alpha} \tag{2}$$

yield

$$M_K \ddot{R}_K^\alpha = -\frac{\partial \mathcal{V}}{\partial R_K^\alpha}, \quad K = 1, \ldots, N;\ \alpha = x, y, z \quad . \tag{3}$$

Let us now introduce a number, n, of holonomic (only coordinate dependent) constraints

$$\sigma_i(\mathbf{R}) = \xi_i(\mathbf{R}) - \xi_i', \quad i = 1, \ldots, n \tag{4}$$

where the $\xi_i(\mathbf{R})$ are geometric variables, e.g. bond lengths, bond angles, or dihedral angles, and the ξ_i' are their respective prescribed values. The Lagrangian of the constrained system is

$$\mathcal{L}' = \mathcal{L} - \sum_i^n \lambda_i \sigma_i \tag{5}$$

with a set of n undetermined Lagrange multipliers λ_i. The corresponding equations of motion are

$$\frac{\partial}{\partial t}\frac{\partial \mathcal{L}'}{\partial \dot{R}_K^\alpha} = \frac{\partial \mathcal{L}'}{\partial R_K^\alpha} \tag{6}$$

or

$$M_K \ddot{R}_K^\alpha = -\frac{\partial \mathcal{V}}{\partial R_K^\alpha} - \sum_i^n \lambda_i \frac{\partial \sigma_i}{\partial R_K^\alpha}, \quad K = 1, \ldots, N;\ \alpha = x, y, z \quad . \tag{7}$$

A commonly used iterative scheme to solve the constrained equations of motion (Eq. (7)) in combination with the Verlet propagation algorithm has been named SHAKE[25,29]. Alternatively, constrained dynamics may be formulated within the Hamiltonian framework[30] in which case one can derive the RATTLE algorithm[31] to be used in conjunction with the velocity Verlet propagator.

2.1.2 Free Energy by Thermodynamic Integration

The free energy difference between two states, ξ^1 and ξ^2, can be expressed in terms of the reversible work required to move from ξ^1 to ξ^2 along the reaction coordinate ξ[13,27,32,33,28]

$$\Delta W = W(\xi^2) - W(\xi^1) = \int_{\xi^1}^{\xi^2} d\xi' \left\langle \frac{\partial \mathcal{H}}{\partial \xi} \right\rangle_{\xi'}^{\text{cond.}} \tag{8}$$

where mean force

$$\left\langle \frac{\partial \mathcal{H}}{\partial \xi} \right\rangle_{\xi'}^{\text{cond.}} = \frac{\left\langle \frac{\partial \mathcal{H}}{\partial \xi} \delta(\xi - \xi') \right\rangle}{\langle \delta(\xi - \xi') \rangle} \tag{9}$$

is the conditional ensemble average evaluated at $\xi = \xi'$ of the generalized force, i.e. the derivative of the Hamiltonian $\mathcal{H}$ with respect to the reaction coordinate ξ.

Using the so-called blue moon ensemble method[26] it is possible to calculate conditional averages from time averages over constrained MD trajectories at fixed values $\xi = \xi'$,

$$\left\langle \frac{\partial \mathcal{H}}{\partial \xi} \right\rangle_{\xi'}^{\text{cond.}} = \frac{\left\langle Z^{-\frac{1}{2}} \left[\frac{\partial \mathcal{V}}{\partial \xi} - kT \frac{\partial \ln |\mathbf{J}|}{\partial \xi} \right] \right\rangle_{\xi'}}{\left\langle Z^{-\frac{1}{2}} \right\rangle_{\xi'}} \tag{10}$$

where the factor

$$Z = \sum_K^N \frac{1}{M_K} \left(\frac{\partial \xi}{\partial \mathbf{R}_K} \right)^2 \tag{11}$$

corrects for the configurational bias introduced by the constraint. The Jacobian matrix, **J**, for the coordinate transformation from Cartesian coordinates, **R**, to generalized coordinates, **u**, including the reaction coordinate ξ, $\mathbf{R} \leftrightarrow u \equiv \{\xi, \mathbf{q}\}$, is defined by

$$J^{\alpha}_{K\kappa} = \frac{\partial R^{\alpha}_{K}}{\partial u_{\kappa}} \quad . \tag{12}$$

In practice, the rhs of Eq. (10) is difficult to evaluate because of the derivatives with respect to ξ. The problem can be simplified considerably by exploiting the fact that the Lagrange multiplier associated with the constraint (cf. Eq. (5)) is equal to the generalized force[34],

$$-\frac{\partial \mathcal{H}}{\partial \xi} = \lambda \quad . \tag{13}$$

This immediately follows from the Hamiltonian equation of motion

$$\dot{p}^{\xi} = -\frac{\partial \mathcal{H}}{\partial \xi} - \lambda \tag{14}$$

realizing that the momentum conjugate, $\dot{p}^{\xi}$, to the constrained variable ξ vanishes. Applying the blue moon unbiasing procedure, the mean force (Eq. (9)) can be expressed in terms of the constrained average of the Lagrange multiplier[27,13,32,33,28],

$$\left\langle \frac{\partial \mathcal{H}}{\partial \xi} \right\rangle^{\text{cond.}}_{\xi'} = \frac{\langle Z^{-\frac{1}{2}}(\lambda - kTG)\rangle_{\xi'}}{\langle Z^{-\frac{1}{2}}\rangle_{\xi'}} \tag{15}$$

with

$$G = \frac{1}{Z^2} \sum_{K,L}^{N} \frac{1}{M_K M_L} \frac{\partial \xi}{\partial \mathbf{R}_K} \frac{\partial^2 \xi}{\partial \mathbf{R}_K \partial \mathbf{R}_L} \frac{\partial \xi}{\partial \mathbf{R}_L} \quad . \tag{16}$$

2.2 Specific Reaction Coordinates

2.2.1 Coordination Constrained Molecular Dynamics

For the study of chemical reactions in solutions, the coordination number of a specific atom $K = C$,

$$\xi = n_C(\mathbf{R}) = \sum_{K \neq C}^{N} \left[\exp[\kappa(r_K - r_c)] + 1\right]^{-1} \tag{17}$$

has proven particularly useful[13]. Here, r_K is the distance of atom K from atom C; the coordination radius r_c and the width of the Fermi function κ are parameters to be set prior to the simulation.

This coordination constraint has been applied in a number of CP-MD studies of proton transfer[14–16,12,35] mostly in aqueous solution. In the following, we shall discuss the example of $P(OH)_5$ in liquid water[15,16].

The study of pentacoordinated phosphorus compounds has played a key role in the attempt to unravel the mechanism of the hydrolysis reaction of RNA[36–39,15]. Experimental evidence on the first step of RNA hydrolysis — so-called cleavage transesterification — has suggested two possible reaction pathways involving a monoanionic phosphorane

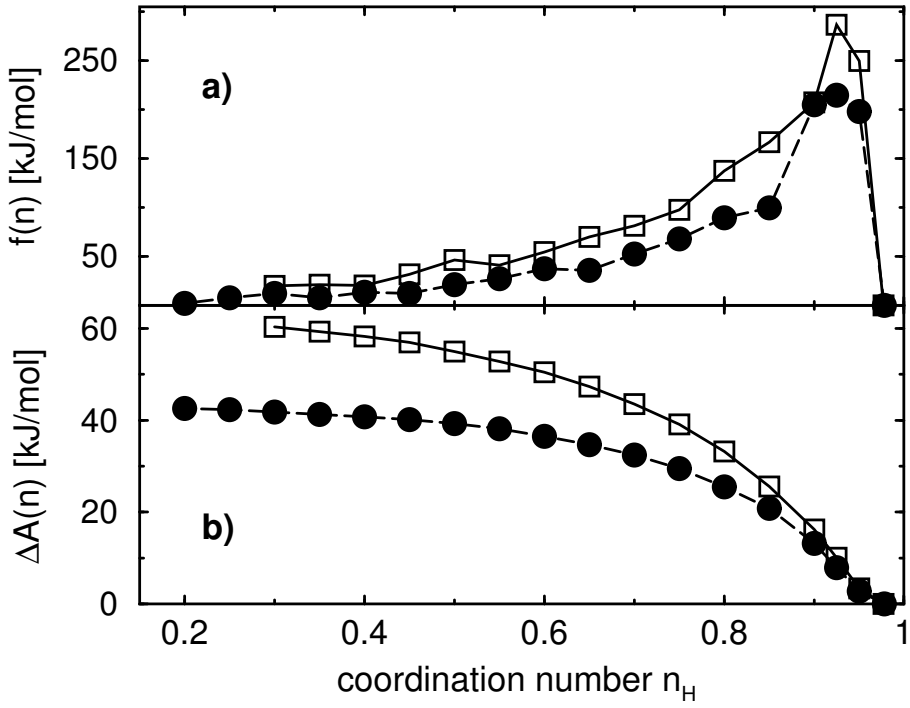

Figure 1. a) Mean force of constraint as a function of the coordination number n for the axial (□) and the equatorial (•) site b) corresponding free energy curves obtained by integration of the mean forces.

transition state and a dianionic phosphorane intermediate, respectively[37,38]. Determination of the phosphorane's lifetime and protonation state is, therefore, of prime importance in establishing a detailed picture of the hydrolysis reaction mechanism. Knowledge of the relevant pK_a values would thus provide vital clues.

The essential quantity required in order to calculate the pK_a value of a given molecule is the Helmholtz free energy difference, ΔA, for hydrogen abstraction. This quantity can be extracted from constrained molecular dynamics by thermodynamic integration provided the control parameter is a reasonable approximation to the reaction coordinate. In high dimensional systems, a simple distance constraint often yields a rather poor approximation to the true reaction coordinate, and when used to locate transition states can lead to erroneous results[40,4]. Simple geometric order parameters, however, can still be suitable as integration variables for the determination of free energy difference between well defined reactant and product states distance. An additional problem is encountered in protic solutions; when the dissociating proton has reached a critical distance from its donor atom, the latter is vulnerable to reprotonation by a different solvent proton. This difficulty is circumvented if we enforce deprotonation by gradually decreasing the coordination number of the oxygen atom of a specific hydroxyl group.

In two separate series of coordination constrained CP-MD simulations, we have determined the free energy for deprotonation of an axial and an equatorial hydroxyl group of

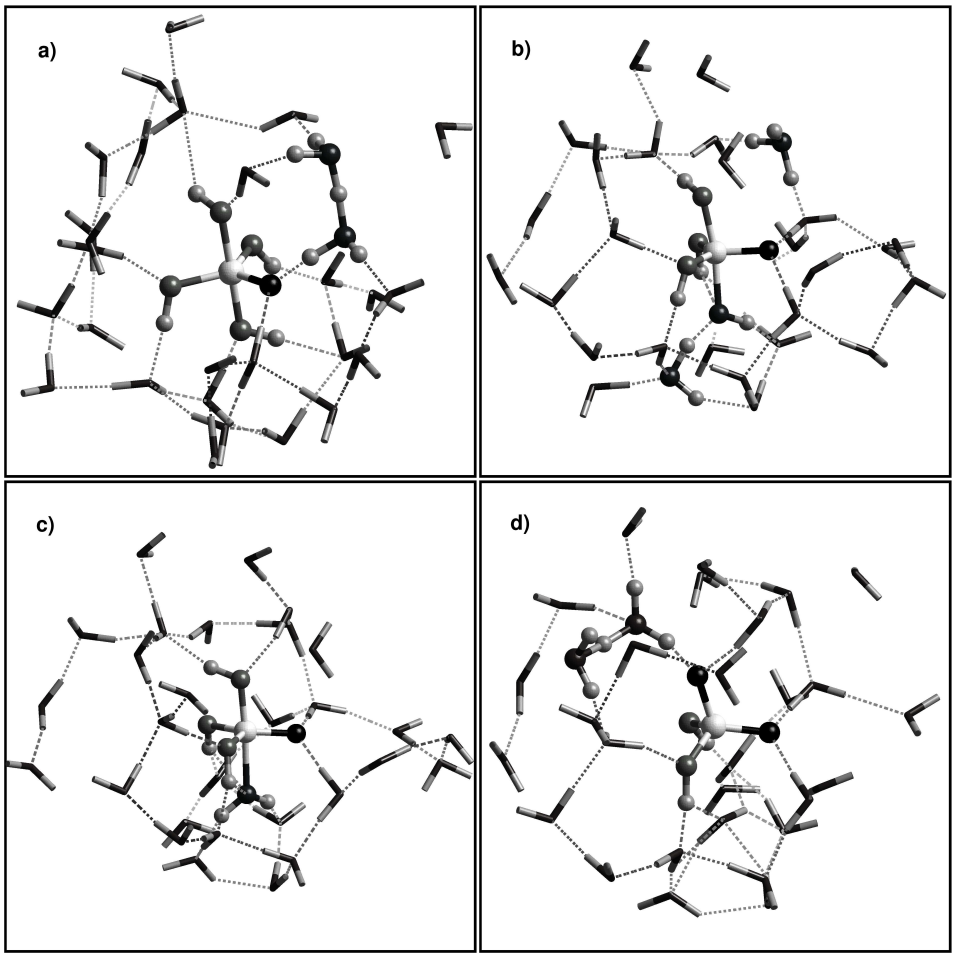

Figure 2. Sequence of snapshots illustrating a dehydration event: a) application of coordination constraints leads to the formation of $H_5O_2^+$. b) a H_3O^+ ion breaks loose and subsequently donates a proton to the axial hydroxyl group of the phosphorane through a chain reaction of proton transfers. c) the axial hydroxyl group has been protonated and is about to break its PO bond. d) the remaining phosphoric acid loses a proton to the solvent.

the trigonally bipyramidal $P(OH)_5$ respectively. The value of n (cf. Eq. (17)) was gradually decreased towards zero starting near its equilibrium value of approximately unity, thus transferring a proton from the hydroxyl group O_DH to the acceptor solvent water molecule H_2O_A. For each, fixed, value of the coordination number a trajectory of roughly 2 to 3 ps length was computed. In Figure 1a the blue-moon corrected average constraint force (Eq. (15)), i.e. the mean force, is plotted as a function of the coordination number for both the axial and the equatorial site. The equilibrium value of n was determined to be 0.98 in both cases from the trajectory of unconstrained $P(OH)_5$. In the region just below the equilibrium value of n we observe a steep rise of the mean force reaching a maximum at $n = 0.925$. As expected, the restoring force resisting proton abstraction is

significantly higher for an axial proton than for an equatorial proton, the mean forces being 286.6 kJ/mol and 214.6 kJ/mol, respectively. With further decreasing coordination number the mean force is seen to fall off towards zero and we observe the formation of a $H_5O_2^+$ ion (Zundel ion) (Figure 2a). The smallest value of n for which a meaningful trajectory could be obtained was 0.2 in the case of the equatorial site and 0.3 for the axial position. For smaller n the $H_5O_2^+$ ion breaks up into a hydronium ion and a water molecule H_2O_A which has accepted the proton from the phosphorane and donated another proton to its nearest neighbor. The newly created H_3O^+ ion is now free to attack the negatively charged phosphorane. Figure 2b-c illustrates how an axial hydroxyl group of the phosphorane is protonated turning it into a H_2O^+ group initially. The corresponding PO bond is subsequently broken and a neutral water molecule leaves the phosphorane molecule. Since we are now dealing with phosphoric acid, H_3PO_4, in water, it is not surprising that we observe spontaneous deprotonation within femtoseconds (Figure 2d). This dehydration process is in competition with the deprotonation reaction we intend to enforce by using coordination constraints and makes it impossible to calculate any trajectories at very small values of n without dissociation of the phosphorane.

The free energy difference ΔA between two values of the coordination number can be obtained by integration of the mean force. In Figure 1b the resulting free energy curves for axial and equatorial hydroxyl groups are plotted taking equilibrium as the reference point. The equatorial curve ends at a free energy difference of 42.7 kJ/mol for $n = 0.2$ well below the axial curve ending at $\Delta A = 60.2$ kJ/mol for $n = 0.3$. Following the procedure outlined in Refs. 15, 16 we have then determined the pK_a values to be 9.8 and 14.2 for equatorial and axial hydroxyl groups, respectively. Very recent experimental estimates based on a bond length – pK_a correlation[41] give 8.62 ± 1.87 and 13.5 ± 1.5 for the equatorial and axial OH groups of tetracyclohexyloxyhydroxyphosphorane[15]. The value of 7.9 calculated by Lopez et al.[39] from an empirical reaction field model for the equatorial OH group of ethylene phosphorane is substantially lower than our estimate. As we have pointed out above, however, explicit treatment of the solvent may make a crucial difference in the current context. Moreover, we should bear in mind that all three pK_a estimates compared here have been obtained for *different* (although in many respects certainly similar) phosphoranes.

2.2.2 Targeted Molecular Dynamics

A detailed description of Targeted MD (TMD) including a discussion of the mechanical and statistical properties of the constraint is available in the literature[9–11]. Here, we simply provide a brief outline including the most important equations.

In TMD, the reaction coordinate is defined as the target distance

$$D(\mathbf{R}) = \sqrt{\sum_{K=1}^{N} \frac{M_K}{M} (\mathbf{R}_K - \mathbf{T}_K)^2} \tag{18}$$

between the instantaneous reactant structure $\mathbf{R} = \mathbf{R}(t)$ and the fixed product (target) structure $\mathbf{T} = \{\mathbf{T}_K\}$, where M is the total mass of the system. In order to eliminate any translational or rotational contributions, the target distance $D(\mathbf{R})$ is minimized by superimposing the centres-of-mass of the two configurations, $\mathbf{R}$ and $\mathbf{T}$, followed by rotation of

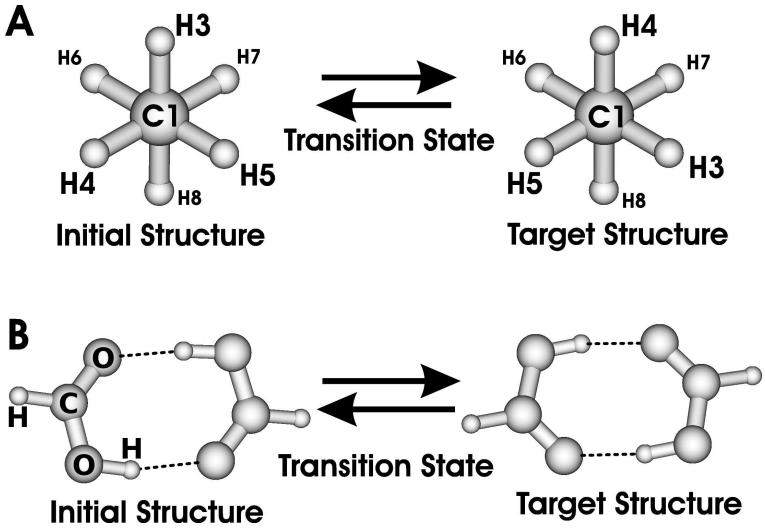

Figure 3. (A) Initial and target ethane structures using the staggered conformation (rotation by 120°) as the target structure (see text for more details). (B) Initial and target FAD structures.

the target structure. The remaining distance, called the target distance, is a measure of the structural root mean square distance between the two molecular conformations. During the course of the molecular dynamics simulation, this distance is gradually reduced towards zero and the initial reactant structure is driven towards the target structure.

A particularly attractive feature of this approach is the fact that the time averaged constraint force (Eq. (15)) can be obtained from a TMD run at a fixed value of D as the average Lagrange multiplier, i.e.

$$\left\langle \frac{\partial \mathcal{H}}{\partial \xi} \right\rangle_{\xi'}^{\text{cond.}} = \langle \lambda \rangle_{\xi'} \tag{19}$$

without the need to correct for metric tensor effects.

TMD using classical force fields has recently been employed with considerable success to study conformational transitions and folding in proteins[42–47]. In the following, however, we will present results from the first TMD study based on Car-Parrinello MD (T-CP-MD). In this study, two test cases were considered, rotation of ethane about the C–C bond and double proton transfer (DPT) in formic acid dimer (FAD). Figure 3 provides a pictorial representation of the initial and target structures for the two systems investigated by T-CP-MD.

The average constraint force for the staggered-to-eclipsed-to-staggered conformational transition (rotation by 120°) in ethane is shown in Figure 4 as a function of the target distance including the associated free energy profile. The initial target distance between the two staggered conformations is $D = 0.88$ a.u. corresponding to a rotational angle about the C–C axis of 120°. At this initial D, the average constraint force is approximately zero. As D decreases, the constraint force increases as the constraint pushes the system towards the energetically unfavourable eclipsed conformation (rotation by 60°). Having

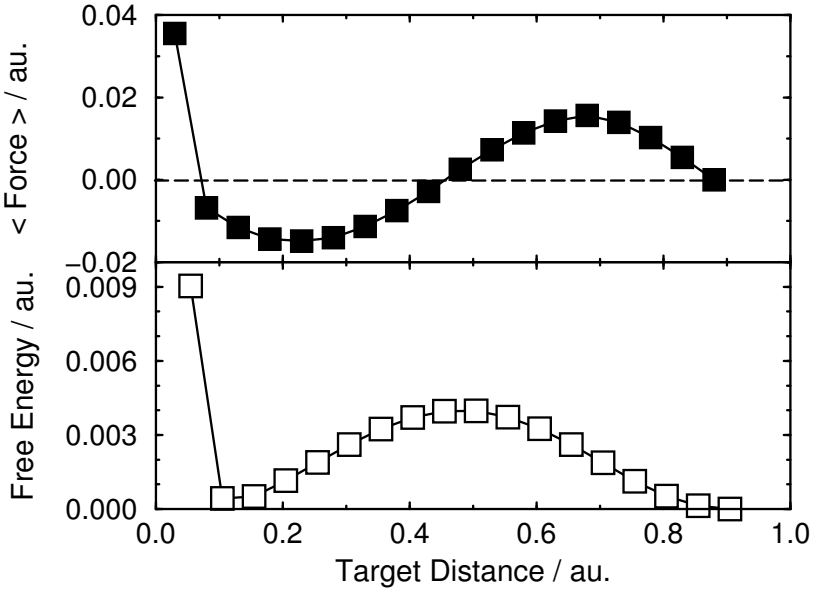

Figure 4. Variation of the average constraint force (top) and free energy profile (bottom) as a function of D for the staggered–eclipsed–staggered transition in ethane using T-CP-MD; see Figure 3(A).

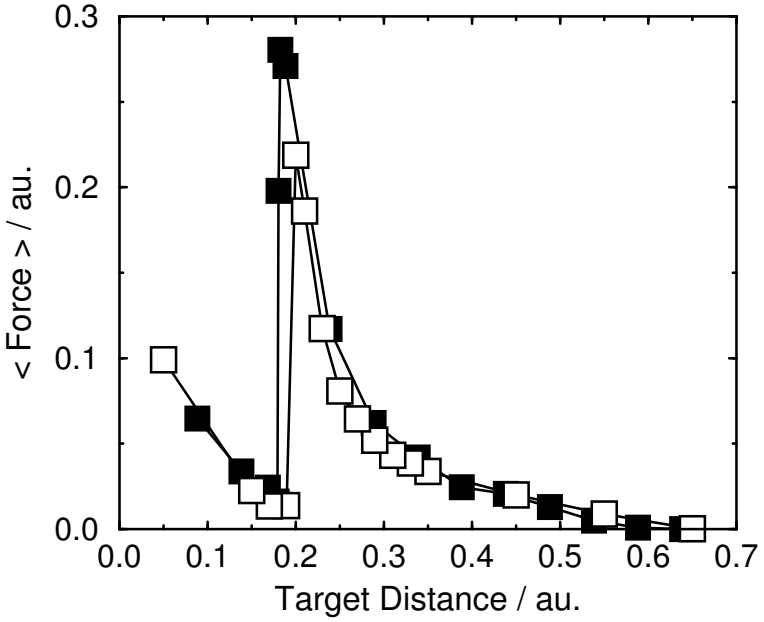

Figure 5. Variation in the average constraint force as a function of D for FAD. Filled squares represent the average constraint force for the 'full' TMD, while the open squares show the result for the partial target structure involving only the four oxygen atoms and the two protons involved in DPT. After the DPT event ($D = 0.2$ a.u.) the constraint loses control of the system.

reached a maximum, the average constraint force then returns to zero at the transition state ($D = 0.43$ a.u.). At this point, the system is sitting exactly on the top of the potential energy barrier. Further reduction of D results in negative values of the average constraint force. This arises from the fact that, having overcome the energy barrier, the system would preferentially move directly to the eclipsed (target) structure. The constraint however does not allow this, and acts in such a way as to "hold" the system away from the target structure, resulting in a negative average constraint force. As D gets very close to zero (in this case for $D < 0.1$ a.u.), the average force adopts exceedingly large positive values. This is because the phase space volume available to the system decreases with D resulting in an increasing centrifugal component of the constraint force[10]. In other words, when the available phase space becomes so small that it confines the vibrations of the system, the average constraint force increases dramatically as a result of this "entropy loss". The free energy profile resembles a Gaussian form, with a maximum at approximately the midpoint of the reaction coordinate. Indeed the resulting free energy profile is very similar to that obtained from the MEP.

For the study of DPT in FAD, we performed two series of T-CP-MD simulations. In the first series of simulations we used a 'full' target constraint including all atoms of the molecule, whilst in the second simulation we employed a "partial" target constraint, only using for the evaluation of D those atoms that are predominantly involved in the DPT reaction, i.e. the four oxygen atoms and two protons constituting the two H-bonds. The resulting average constraint force curves are depicted in Figure 5. In both cases, we see a very different force curve compared to that obtained in the ethane simulation. The average constraint force increases slowly to a maximum as the DPT event is reached. Just after DPT, the average constraint force rapidly decreases to zero. At very small D, the average constraint force begins to increase again, due to the effect of the target constraint entropy. It is immediately apparent that in FAD, the constraint "loses control" of the system after the DPT reaction has occurred. We consider that this is partially due to the fact that FAD is much more flexible than ethane and partially due to the fact that the TMD constraint is not "focussed" directly on the protons involved in DPT, that is the mass-weighted target distance is dominated by the heavy atom frame.

3 Metadynamics

Another common strategy to accelerate barrier crossings consists in modifying the potential energy landscape in such a way as to "fill up" potential minima[48–50,17,51,52]. In this section, we will describe a particular method of this type which has been named metadynamics[20–24,53].

Prior to the simulation one has to define a number, n, of reaction coordinates $\xi_i(\mathbf{R})$ characterizing the transitions between several local minima of the potential energy surface. For each reaction coordinate ξ_i an associated dynamical variable Ξ_i is introduced, component of the vector $\boldsymbol{\Xi}$. The Lagrangian of the extended system is

$$\tilde{\mathcal{L}} = \mathcal{L} + \frac{1}{2}\sum_i^n \mu_i \dot{\Xi}_i^2 - \frac{1}{2}\sum_i^n k_i \left[\xi_i(\mathbf{R}) - \Xi_i\right]^2 - V(t, \boldsymbol{\Xi}) \tag{20}$$

where $\mathcal{L}$ is the standard Lagrangian underlying the MD, in the simplest case (Eq. (1)), μ_i and k_i are the fictitious mass and the coupling constant associated with the reaction

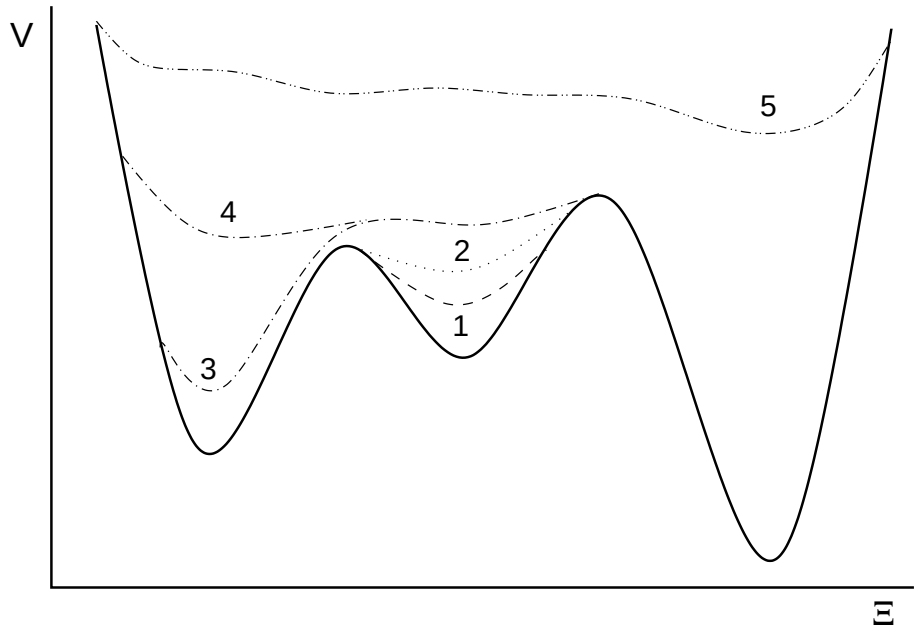

Figure 6. Schematic illustration of the metadynamics history-dependent potential $V(t, \mathbf{\Xi})$ as a function of time (curves labelled 1–5 in the order of increasing simulation time) added to the potential energy surface (solid line). The simulation started in the central minimum before the system is driven to the left minimum and finally to the minimum on the right.

coordinate ξ_i. The history-dependent biasing potential is defined as

$$V(t, \mathbf{\Xi}) = \sum_{t_k < t} W_k \exp\left[-\frac{(\mathbf{\Xi} - \mathbf{\Xi}^k)^2}{2(\Delta\Xi^\perp)^2}\right] \exp\left[-\frac{[(\mathbf{\Xi}^{k+1} - \mathbf{\Xi}^k)(\mathbf{\Xi} - \mathbf{\Xi}^k)]^2}{2(\Delta\Xi_k^\parallel)^4}\right] \qquad (21)$$

with $\mathbf{\Xi} = \mathbf{\Xi}(t)$ and $\mathbf{\Xi}^k = \mathbf{\Xi}(t_k)$; $\Delta\Xi_k^\parallel = |\mathbf{\Xi}^{k+1} - \mathbf{\Xi}^k|$ and $\Delta\Xi^\perp$ determine the width of the Gaussian in the direction perpendicular and parallel to the motion of $\mathbf{\Xi}$. In earlier publications on metadynamics[21,22], the prefactor W_k was updated according to

$$W_k = \lambda \sum_i^n (\Xi_i^{k+1} - \Xi_i^k) \langle k_i \left[\xi_i(\mathbf{R}) - \Xi_i\right] \rangle \qquad (22)$$

counterbalancing the restoring force contribution from the free energy surface. The average $\langle\rangle$ is taken over the time interval $\Delta t = t_{k+1} - t_k$ (typically 10–100 times larger than the MD time step) between two updates of the potential $V(t, \mathbf{\Xi})$ and λ is chosen smaller than unity[21]. In some recent works, a constant prefactor $W_k = W$ was found to be more advantageous[53,24].

As the simulation time approaches infinity, the history-dependent potential $V(t, \mathbf{\Xi})$ has filled all the potential wells of the free energy surface and represents the negative of the latter, i.e., using the same notation as above (cf. Eq. (8)),

$$\lim_{t\to\infty} V(t, \mathbf{\Xi}) = -W(\mathbf{\Xi}) + \text{const.} \qquad (23)$$

A schematic one-dimensional illustration of the time evolution of the biasing potential $V(t, \boldsymbol{\Xi})$ for a typical potential energy surface can be seen in Figure 6. The Gaussian-shaped potential hills (Eq. (21)) drive the system away from previously visited regions of configuration space. This occurs in an indirect way by propagating the fictitious dynamical variables Ξ_i to which the actual reaction coordinates $\xi_i(\mathbf{R})$ are coupled through the third (harmonic) term on the rhs of Eq. (20). The parameters μ_i, k_i, W, and $\Delta\Xi^{\perp}$ have to be chosen carefully to ensure efficient and, at the same time, accurate exploration of the free energy surface. The width $\Delta\Xi^{\perp}$ of the Gaussian hills can be estimated from fluctuations of the Ξ_i in the unbiased potential, i.e. $V(t, \boldsymbol{\Xi}) = 0$. The height of the individual hills, W, should be lower than kT. The fictitious masses, μ_i, and the spring constants, k_i, have to chosen in such a way as to keep the Ξ_i close to the reaction coordinates $\xi_i(\mathbf{R})$ while maintaining adiabatic separation of fictitious and nuclear degrees of freedom.

Acknowledgements

I am grateful to Dominik Marx, Michiel Sprik, Jürgen Schlitter, Phineus Markwick, and Nisanth Nair for helpful discussions.

References

1. R. Car and M. Parrinello. *Phys. Rev. Lett.*, 55:2471, 1985.
2. D. Marx and J. Hutter. In J. Grotendorst, editor, *Modern Methods and Algorithms of Quantum Chemistry*. NIC, Jülich, 2000. `www.theochem.rub.de/go/cprev.html`.
3. D. Chandler. In B. J. Berne, G. Ciccotti, and D. F. Coker, editors, *Classical and Quantum Dynamics in Condensed Phase Simulations*. World Scientific, Singapore, 1998.
4. P. G. Bolhuis, D. Chandler, C. Dellago, and P. L. Geissler. *Ann. Rev. Phys. Chem.*, 53:291, 2002.
5. L. R. Pratt. *J. Chem. Phys.*, 85:5045, 1986.
6. P. L. Geissler, C. Dellago, D. Chandler, J. Hutter, and M. Parrinello. *Science*, 291:2121, 2001.
7. A. Curioni, M. Sprik, W. Andreoni, H. Schiffer, J. Hutter, and M. Parrinello. *J. Am. Chem. Soc.*, 119:7218, 1997.
8. E. J. Meijer and M. Sprik. *J. Am. Chem. Soc.*, 120:6345, 1998.
9. J. Schlitter, M. Engels, P. Krüger, E. Jacobi, and A. Wollmer. *Mol. Sim.*, 10:291, 1993.
10. J. Schlitter, W. Swegat, and T. Mülders. *J. Mol. Mod.*, 7:171, 2001.
11. J. Schlitter and M. Klähn. *Mol. Phys.*, 101:3439, 2003.
12. P. Markwick, N. L. Doltsinis, and D. Marx. *J. Chem. Phys.*, 122:054112, 2005.
13. I. Shavitt. *Mol. Phys.*, 94:3, 1998. and references therein.
14. M. Sprik. *Chem. Phys.*, 258:139, 2000.
15. J. E. Davies, N. L. Doltsinis, A. J. Kirby, C. D. Roussev, and M. Sprik. *J. Am. Chem. Soc.*, 124:6594, 2002.
16. N. L. Doltsinis and M. Sprik. *Phys. Chem. Chem. Phys.*, 5:2612, 2003.

17. E. M. Müller, A. de Meijere, and H. Grubmüller. *J. Chem. Phys.*, 116:897, 2002.
18. J. VandeVondele and U. Röthlisberger. *J. Phys. Chem. B*, 106:203, 2002.
19. L. Rosso and M. E. Tuckerman. *Mol. Sim.*, 28:91, 2002.
20. A. Laio and M. Parrinello. *Proc. Natl. Acad. Sci. USA*, 99:12562, 2002.
21. M. Iannuzzi, A. Laio, and M. Parrinello. *Phys. Rev. Letters*, 90:238302, 2003.
22. A. Stirling, M. Iannuzzi, A. Laio, and M. Parrinello. *ChemPhysChem*, 5:1558, 2004.
23. A. Laio, A. Rodriguez-Fortea, F. L. Gervasio, M. Ceccarelli, and M. Parrinello. *J. Phys. Chem. B*, 109:6714, 2005.
24. B. Ensing, A. Laio, M. Parrinello, and M. L. Klein. *J. Phys. Chem. B*, 109:6676, 2005.
25. J. P. Ryckaert, G. Ciccotti, and H. J. C. Berendsen. *J. Comp. Phys.*, 23:327, 1977.
26. E. A. Carter, G. Ciccotti, J. T. Hynes, and R. Kapral. *Chem. Phys. Lett.*, 156:472, 1989.
27. M. Sprik and G. Ciccotti. *J. Chem. Phys.*, 109:7737, 1998.
28. G. Ciccotti and M. Ferrario. *Mol. Sim.*, 30:787, 2004.
29. G. Ciccotti and J. P. Ryckaert. *Comp. Phys. Rep.*, 4:345, 1986.
30. S. W. Deleeuw, J. W. Perram, and H. G. Petersen. *J. Stat. Phys.*, 61:1203, 1990.
31. H. C. Andersen. *J. Comp. Phys.*, 52:24, 1983.
32. G. Ciccotti and M. Ferrario. *J. Mol. Liq.*, 89:1, 2000.
33. I. Coluzza, M. Sprik, and G. Ciccotti. *Mol. Phys.*, 101:2885, 2003.
34. T. Mülders, P. Krüger, W. Swegat, and J. Schlitter. *J. Chem. Phys.*, 104:4869, 1996.
35. H. Langer, N. L. Doltsinis, and D. Marx. *ChemPhysChem*, 6:1734, 2005.
36. F. H. Westheimer. *Acc. Chem. Res.*, 1:70, 1968.
37. M. Oivanen, S. Kuusela, and H. Lonnberg. *Chem. Rev.*, 98:961, 1998.
38. D. M. Perreault and E. V. Anslyn. *Angew. Chem. Int. Ed. Engl.*, 36:432, 1997.
39. X. Lopez, M. Schneider, A. Dejaegere, and M. Karplus. *J. Am. Chem. Soc.*, 124:5010, 2002.
40. C. Dellago, P. G. Bolhuis, F. S. Csajka, and D. Chandler. *J. Chem. Phys.*, 108:1964, 1998.
41. R. D. Amos, N. C. Handy, P. G. Jones, A. J. Kirby, J. K. Parker, J. M. Percy, and D. M. Su. *J. Chem. Soc., Perkin Trans.*, 2:549, 1992.
42. B. Wroblowski, J.F. Diaz, J. Schlitter, and Y. Engelborghs. *Prot. Eng.*, 10:1163, 1997.
43. O. Roche and M.J. Field. *Prot. Eng.*, 12:285, 1999.
44. P. Fererra, J. Apostolakis, and A. Calfisch. *J. Phys. Chem. B.*, 104:4511, 2000.
45. P. Fererra, J. Apostolakis, and A. Calfisch. *Proteins*, 39:252, 2000.
46. P. Kruger, S. Verheyden, P.J. Declerck, and Y. Engelborghs. *Prot. Sci.*, 10:798, 2001.
47. Y.K. Kong, Y.F. Shen, T.E. Warth, and J.P. Ma. *Proc. Natl. Acad. Sci. USA*, 99:5999, 2002.
48. H. Grubmüller. *Phys. Rev. E*, 52:2893, 1995.
49. J. VandeVondele and U. Röthlisberger. *J. Chem. Phys.*, 113:4863, 2000.
50. J.-C. Wang, S. Pal, and K.-A. Fichthorn. *Phys. Rev. B*, 63:085403, 2001.
51. J. A. Rahman and J. C. Tully. *Chem. Phys.*, 285:277, 2002.
52. D. Hamelberg, J. Mongan, and J. A. McCammon. *J. Chem. Phys.*, 120:11919, 2004.
53. K. Jug, N. N. Nair, and T. Bredow. *Phys. Chem. Chem. Phys.*, 7:2616, 2005.